1

ZnO Nanorods Arrays and Heterostructures for the High Sensitive UV Photodetection

Soumen Dhara and P. K. Giri
Department of Physics, Indian Institute of Technology Guwahati, Guwahati, India

1. Introduction

In the field of semiconductor nanostructures, one–dimensional (1D) ZnO nanostructures (*e.g.* Nanowires, nanorods, nanobelts) are the most promising candidates due to their important physical properties and application prospects. Large surface–to–volume ratio and direct carrier conduction path of 1D ZnO nanostructures are the key factors for getting edge over other types of nanostructures. ZnO is a direct wide band gap materials having bandgap of ~3.37 eV and high excitonic binding energy, 60 meV at room temperature. 1D ZnO nanostructures are extensively studied for their applications in various electronic and optoelectronic devices, e.g., field effect transistors, ultra violet (UV) photodetectors, UV light emitting diodes, UV nanolaser, field emitter, solar cells etc.. (Huang et al., 2001a; Liao et al., 2007; Li et al., 2005; Kind et al., 2002; Soci et al., 2007; Alvi et al., 2010; Liu et al., 2009; Law et al., 2005; Law et al., 2006; Yeong et al., 2007; Xu et al., 2010; Gargas et al., 2009) Various types of ZnO nanorods (NRs) have been grown by several groups worldwide (Huang et al., 2001b; Wei et al., 2010; Ahn et al., 2004; Li et al., 2008; Dhara & Giri, 2011c; Chen et al., 2010; Giri et al., 2010) and they studied the effect of growth conditions on the morphology of the ZnO NRs. The surface of the nanostructures has crucial role in determining the electrical and optoelectronic properties of nano-devices. As the surface-to-volume ratio in NRs is very high, the surface states also play a key role on optical absorption, luminescence, photodetection and other properties. Thus, nanoscale electronic devices have the potential to achieve higher sensitivity and faster response than the bulk material.

Since the first report on UV photodetection from single ZnO nanowires by Kind et al. (Kind et al., 2002), many efforts have been made on 1D ZnO, including NRs to improve the photodection and photoresponse behaviours. It is known that, photodetection and photoresponse of the ZnO NRs depends on the surface condition, structural quality, methods of synthesis and rate of oxygen adsorption and photodesorption. Therefore, it is expected that arrays of NRs, surface modification or structural improvement can enhance the photosensitivity as well as photoresponse. In the steps towards this goal, various groups have put efforts to enhance the photoresponse and photosensitivity by using appropriate dopant, structural improvement, surface passivation, peizo-phototronic effect and making heterostructures with suitable organic or inorganic materials (Porter et al., 2005; Bera & Basak, 2010; Dhara & Giri, 2011a; Liu et al., 2010a; Yang et al., 2010; Chang et al., 2011). However, photosensitivity value and photoresponce time of the ZnO NWs based

photodetectors will require significant improvements in order to meet future demands in variety of fields. At the same time it is also more important to understand the origin of improvement in the photodetection behaviours from ZnO NRs heterostructures in order to play with the photodetection properties to make the flexible photodetectors.

In this chapter we will present a review of the recent achievements on the controlled growth of vertically aligned ZnO NRs arrays and heterostructures by our group and other research groups. Then we will describe the basic properties of these arrays for the application of UV photodetection by means of crystal structures, optical absorption, emission, photoresponse, photosensitivity and photocurrent spectra. The effects of arrays and heterostructures on the mechanism of improved photodetection behavior are also discussed.

2. Growth of ZnO nanorods

ZnO is a II-VI group compound semiconductor whose ionic nature in between covalent and ionic semiconductor. Although the crystal structures shared by ZnO are wurtzite, zinc blende, and rocksalt, however at ambient conditions, only wurtzite phase is thermodynamically stable. The wurtzite structure has a hexagonal unit cell with two lattice parameters, a and c, in the ratio of c/a=1.633 and belongs to the space group of C_{6v}^4or $P6_3mc$. The hexagonal lattice of ZnO is characterized by two interconnecting sublattices of Zn^{2+} and O^{2-}, such that each Zn ion is surrounded by a tetrahedral of O ions, and vice-versa. The Zn terminated polar (0001) plane is the primary growth direction due to the lower surface energy of this plane.

ZnO NRs with controlled shape and order could be grown by thermal vapor deposition (TVD) (Huang et al., 2001b; Giri et al., 2010; Li et al., 2008; Yao et al., 2002), metal–organic chemical vapor deposition (Yuan & Zhang, 2004; Park et al., 2002; Kim et al., 2009), molecular beam epitaxy (Heo et al., 2002), hydrothermal/solvothermal methods (Breedon et al., 2009; Verges et al., 1990; Alvi et al., 2010; Tak & Yong, 2005; Pacholski et al., 2002; Song & Lim, 2007) and top down approach by etching (Wu et al., 2004). Among those techniques, vapor deposition and chemical methods are the widely used techniques for their versatility about controllability, repeatability, quality and mass production. MOCVD and MBE can give high quality ZnO NRs arrays, but use of these techniques are limited, due to the poor sample uniformity, low product yield, choices of substrate, and also the high experimental cost. In the vapor deposition method, the growth process follows either vapor–liquid–Solid (VLS) or vapor–solid (VS) mechanisms, depending on the growth conditions. On the other hand, the NWs are grown by chemical reaction with the seed layer in the hydrothermal/solvothermal methods with the assistance of cationic surfactant. In the growth of ZnO NRs, in general metal catalyst or ZnO seed layer are used to promote the one dimensional and vertical growth. In this case catalyst/seed layer act as a nucleation site and facilitate the one–dimensional growth.

2.1 Mechanosynthesis method

Mechanosynthesis method is generally used for the synthesis of binary metal oxide or complex oxide nanocrystals/quantum dots, however recently we successfully synthesized good quality ZnO NRs with varying sizes. Metal nanoparticles (Tsuzuki & McCormick, 2004; Ding et al., 1995), ZnO nanocrystals (Tsuzuki & McCormick, 2001; Ao et al., 2006), CdS

quantum dots (Patra et al., 2011) and various complex oxide nanoparticles (Pullar et al., 2007; Mancheva et al., 2011) have been synthesized by several groups using mechanosynthesis technique. For the growth of the NRs by this method, a suitable surfactant should be chosen, which play a crucial role for the growth in one–direction. The important advantages of this method are NRs can be grown at room temperature and a very fast way, compared to any other chemical methods. In addition, size of NRs could be controlled by reaction time duration and ball to mass ratio.

We have synthesized ZnO NRs of various diameters by mechanosynthesis method at room temperature for reaction time as short as 30 minutes (Chakraborty et al., 2011; Dhara & Giri, 2011b). For the growth of ZnO NRs, mechanochemical reactions were carried out in a planetary ball–milling apparatus. Zinc acetate [$Zn(CH_3COO)_2$], N-cetyl, N, N, N-Trimethyl ammonium bromide (CTAB), a cationic surfactant and sodium hydroxide pellets were used as starting materials. The cationic surfactant plays a crucial role in this reaction and facilitate the growth along only one–direction. The reagents were first mixed together properly before starting milling process. Millings were performed at 300 rpm for the time durations 30 min, 2 and 5 h. After the mechanosynthesis reaction, the resultant product was washed several times by DI water and then with alcohol to remove the surfactant and other bi-products. In the next step, it was dried for 2 h at 100° C to remove the water moister and organic agents.

Figure 1 shows the field emission scanning electron microscope (FESEM) image of the ZnO NRs grown for 30 min reaction, which clearly shows a bundle of dense ZnO NRs. The inset shows the higher resolution isolated NRs of the same sample. The measured diameter and length of the NRs varies in the range 22–45 nm and 300–780 nm, respectively. The FESEM images of the ZnO NRs with reaction time 2 and 5h show similar morphology with smaller lengths in the range 200–600 nm.

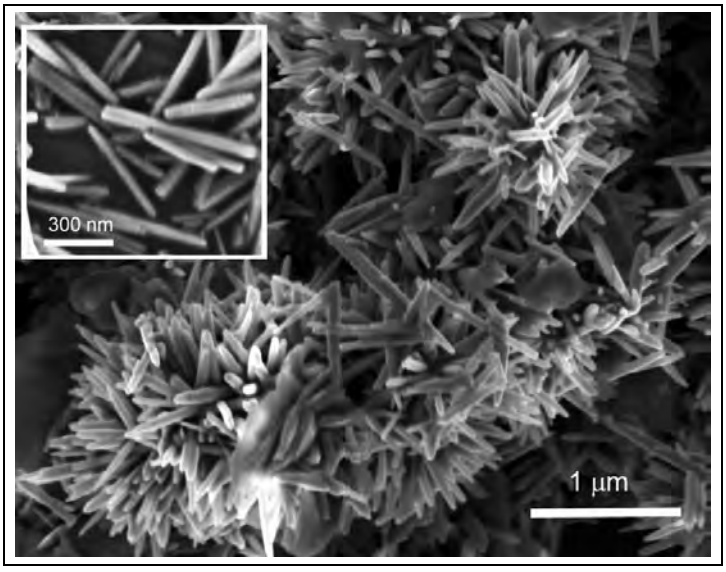

Fig. 1. FESEM image of the ZnO NRs grown for 30 min reaction, agglomerated bundle of ZnO NRs are clearly visible. Inset shows the high resolution image of the isolated NRs.

2.2 Vapor-liquid-solid growth method

Vapor–phase synthesis method is the most extensivly explored method for the growth of one–dimensional nanostructructures. Among all vapor-based methods, the VLS mechanism seems to be the most successful in generating large quantities of nanowires with single crystalline structures. Wagner & Ellis (Wagner & Ellis, 1964) first reported this mechanism in the 1960s to produce micrometer-sized wires, later justified thermodynamically and kinetically by Givargizov in 1975 (Givargizov, 1975). In the early twenty–first century, this mechanism is extensively explored by several research groups worldwide to prepare nanowires and NRs from a rich variety of inorganic materials (Wu & Yang, 2000; Zhang et al., 2001; Wu & Yang, 2001; Gudiksen & Lieber, 2000; Wu et al., 2002b; Duan & Lieber, 2000; Pan et al., 2001; Gao et al., 2003; Chen et al., 2001; Wang et al., 2002b). The VLS growth mechanism is practically demonstrated by Yang group (Wu & Yang, 2001) with the help of in–situ transmission electron microscopy (TEM) techniques by monitoring the VLS growth mechanism in real time. In a typical VLS growth, the growth species is evaporated first, and then diffuses and dissolves into a liquid droplet (catalyst particle). The surface of the liquid has a large accommodation coefficient, and is therefore a preferred site for deposition. Saturated growth species in the liquid droplet will diffuse to and precipitate at the interface between the substrate and the liquid. The precipitation will first follow nucleation and then crystal growth. Continued precipitation or growth will separate the substrate and the liquid droplet, resulting in the growth of nanowires/NRs. Preferential 1D growth continues in the presence of reactant as long as the catalyst nanocluster remains in the liquid droplet state.

2.2.1 Self catalytic seed layer assisted growth

For VLS growth of the NWs, metal catalyst nanoisland/nanocluster is essential. However, undesired metal contamination is generally seen for the NRs grown at relatively lower temperature. For the binary compound, it is possible for one of these elements or the binary compound itself to serve as the VLS catalyst. The nanostructures grown by this process is named as self catalytic growth. The major advantage of a self-catalytic process is that it avoids undesired contamination from foreign metal atoms typically used as VLS catalysts. Different groups have reported the ZnO seed layer assisted catalyst free growth of ZnO NRs and studied its morphology and crystallinity by different methods (Li et al., 2006; Li et al., 2008; Li et al., 2009; Kim et al., 2009). Li et al. synthesized vertically aligned ZnO NRs with uniform length and diameter on silicon substrate by vapor-phase transport method and studied the structure, temperature dependent photoluminescence (PL) and field emission behaviours. In this case ZnO seed layer was prepared by pulsed laser deposition (PLD) technique. Kim et al. (Kim et al., 2009) obtained ZnO NRs by metal-organic chemical vapour deposition method with enhanced aspect ratio at relatively a low temperature (300 °C) by supplying additional Ar carrier gas at a high flow rates. In another work by Feng et al. (Feng et al., 2010), well-crystalline with excellent optical properties, flower-like zinc oxide NRs have been synthesized on Si(111) substrate using a PLD prepared Zn film as "self-catalyst" by the simple thermal evaporation oxidation of the metallic zinc powder at 800 °C. The crystalline quality of the ZnO seed layer strongly controlled the structural quality of the NRs. In most of the cases, synthesized NRs were not aligned, hence have limited applications in nanosize electronic and optoelectronic devices. The precise control over the NRs/nanowires lengths and diameters using a self-catalytic VLS technique is very difficult.

We have synthesized small diameter vertically grown ZnO NRs by self catalytic process using ZnO seed layer. First, high quality thin ZnO seed layer of thickness of 200 nm was deposited on the pre–cleaned, HF etched Si wafer by RF–magnetron sputtering. A mixture of high purity ZnO powder and high purity graphite powder at a weight ratio of 1:1 was used as a source. ZnO vapor was produced inside a horizontal quartz tube at 900°C, which was placed inside the muffle furnace. The ZnO vapor was deposited on the seed layer coated Si substrate in downstream direction at 800°C. The vapor deposition was carried out under the Argon gas flow for 30 min. After deposition the entire system was cooled down to room temperature and the synthesized product was characterized.

Figure 2 shows the ZnO seed layer assisted self catalytically grown ZnO NRs, which were grown vertically on the Si substrate. The diameter of the NRs varies in the range of 100-200 nm with a length up-to 1μm. Although the ZnO NRs are grown vertically but the growth orientation is random. From the FESEM image it is revealed that ZnO seed droplet is present on the top of the NRs. It was reported that the quality and diameters of the ZnO NRs depended on the crystallinity and particle size of the seed layer (Cui et al., 2005; Song & Lim, 2007; Zhao et al., 2005). In our case, the grown NRs are non uniform in diameter and length and also not well aligned due to the non uniform distribution of ZnO seed layer. As a result, these ZnO NRs are not suitable for further use in nanodevices. Then we move to the growth process of ZnO NRs by using a metal catalyst.

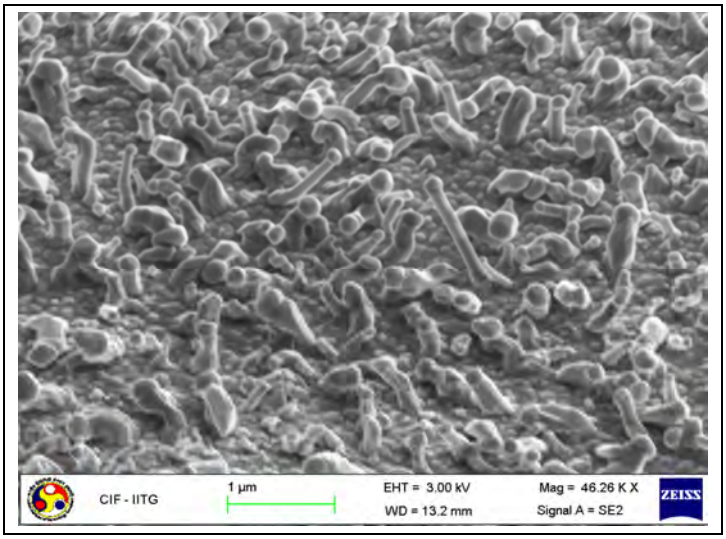

Fig. 2. 45° tilted FESEM image of the seed layer assisted self catalytically grown ZnO NRs.

2.2.2 Gold catalyst assisted growth

For the metal catalyst assisted growth of ZnO NRs, gold catalyst has got major popularity and extensively used due to its comparatively lower eutectic temperature (temperature require to form liquid droplet alloy of Au with the ZnO) and good solvent capability of forming liquid alloy with ZnO. Huang et al. (Huang et al., 2001b) first reported on the

synthesis of highly crystalline ZnO nanowires via VLS growth mechanism using mono–dispersed Au colloid as catalyst. Diameter control of the nanowires was achieved by varying the Au layer thickness. They were also able to synthesized patterned nanowires network by patterning the Au catalyst on the substrate. Later, several groups have synthesized ZnO NRs with varieties of ordering using Au catalyst. He at al. (He et al., 2006), using AFM nanomachining technique together with catalytically activated vapor phase transport and the condensation deposition process, have grown a variety of patterned and featured ZnO NRs arrays. The grown pattern and feature are designed by the dotted catalyst prepared by using AFM tip indentation with controlled location, density, and geometrical shape. The vertical orientation of the NRs is achieved by the epitaxial growth on a single-crystal substrate. This technique allows a control over the location, shape, orientation, and density of the grown NRs arrays. Hejazi et al. (Hejazi & Hosseini, 2007) prepared Au-catalyzed ZnO NRs and studied the growth rate on lateral size of NRs, concentration and supersaturation of Zn atoms in the liquid droplet by a theoretical kinetic model, which is in good agreement with the experimental results. A general expression for the NR growth rate was obtained by materials' balance in the liquid droplet and growth front. Based on the derived formula, growth rate is inversely proportional to nanorod radius. A new understanding of the vapour-liquid-solid process of Au catalyzed ZnO NRs was presented by Kirkham et al. (Kirkham et al., 2007) by studying orientation relationships between the substrates, ZnO NRs and Au particles using x-ray texture analysis. From analysis, they claimed that the Au catalyst particles were solid during growth, and that growth proceeded by a surface diffusion process, rather than a bulk diffusion process. ZnO NRs are also grown successfully on the Si (100) or Al_2O_3 substrates by using Cu or NiO or tin as catalyst (Li et al., 2003; Lyu et al., 2002; Lyu et al., 2003; Wu et al., 2009; Gao et al., 2003).

ZnO NRs were synthesized by vapour deposition method on the Si substrate using Au as catalyst. ZnO vapour was prepared at 900°C from the mixture of commercial ZnO powder and graphite powder. ZnO NRs were grown at 800°C on the Au sputtered (of thickness ~5 nm) Si substrate.

Figure 3 shows the SEM image of the randomly oriented vertically grown ZnO NRs. The hexagonal facet of the ZnO NRs is clearly visible from the image. The diameters of the NRs vary from 100 nm to few hundreds of nm with length about few microns. Although the as-grown NRs are grown vertically but the diameter/length and orientation are not uniform. It is suggested that the non-uniformity is due to the non–uniform grain size of the Au in the sputtered film. It is also believed that lattice mismatch between Si and ZnO is responsible for non–uniform orientation.

2.2.3 Combined seed layer and gold catalyst assisted growth

As discussed before, the seed layer as well as the Au catalyst both failed to produces well–aligned ZnO NRs by vapor transport method. Zhao et al. (Zhao et al., 2005) first used the ZnO buffer layer along with Au catalyst and a well–aligned ZnO NRs is obtained. We also studied the effect of pre-depositing ZnO seed layer on the structure, morphology and optical properties of Au catalytic grown vertically aligned ZnO NRs arrays at different temperatures. (Giri et al., 2010) Based on the obtained results, it is understood that ZnO seed layer and Au layer together acting as the nucleation site and guide the NRs growth. So, for

the Au/ZnO/Si substrate the nucleation sites of ZnO NRs have the same orientation as ZnO thin film by the effect of the seed layer. The catalyst layer transfers the orientation from seed layer to NRs leading to a vertically well–aligned growth (Zhao et al., 2005; Giri et al., 2010).

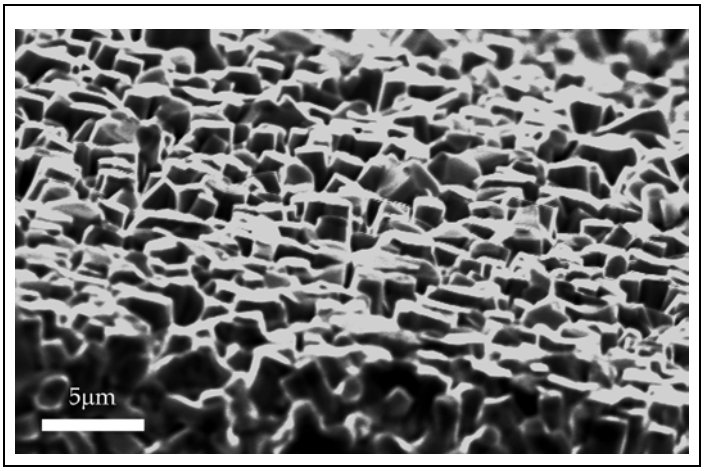

Fig. 3. SEM image of Au catalyst assisted randomly oriented ZnO NRs grown at 800°C.

In the first step of ZnO NRs growth, a ZnO seed layer was deposited by RF-magnetron sputtering followed by deposition of ultrathin Au layer by DC sputtering. Then ZnO NRs were grown in the temperature range of 700-900°C by vapour transport method, as described earlier.

Figure 4 shows typical SEM morphology of ZnO NRs grown on Au/ZnO/Si substrate at various growth temperatures. The NRs grew vertically on the substrate at 900°C, as seen from Fig. 2(a). The sizes of the NRs are in the range of few hundred nanometers and non-uniform diameters are due to variation in the local thickness of ZnO seed layer. ZnO seeds act as a nucleation sites for the NRs growth and importantly offers very negligible lattice mismatch or almost mismatch free interface between seed layer and NRs, which results in the high quality vertically aligned growth of ZnO NRs arrays. NRs grown at 900 and 850°C have larger diameter and highly aligned as comparable to the NRs grown at 700°C.

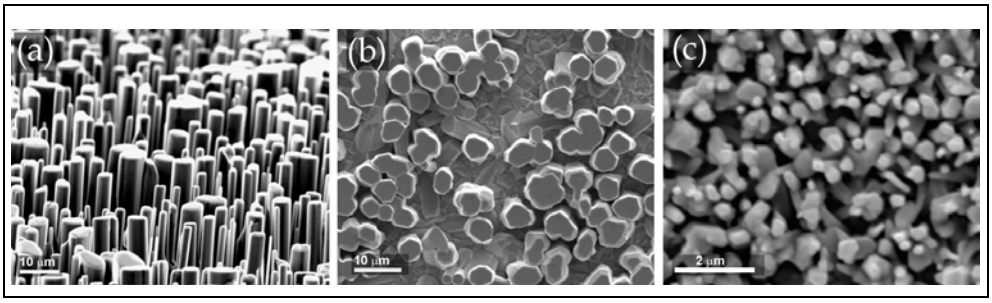

Fig. 4. SEM images of seeded layer and Au catalyst assisted grown aligned ZnO NRs grown at different substrate temperatures: (a) 900°C, (b) 850°C, (c) 700°C, respectively.

2.3 Aqueous chemical growth

Aqueous chemical growth methods are attractive for several reasons: low cost, less hazardous, and thus capable of easy scaling up; growth occurs at a relatively low temperature, compatible with flexible organic substrates; there is no need for the use of metal catalysts; in addition, there are a variety of parameters that can tuned to effectively control the morphologies and properties of the final products (Pearton et al., 2005; Xu et al., 2009; Guo et al., 2011b). The growth process ensures that a majority of the NRs in the array are in direct contact with the substrate and provide a continuous pathway for carrier transport, an important feature for future electronic devices based on these materials. Aqueous chemical methods have been demonstrated as a very powerful technique for the growth of 1D ZnO nanostructures via selective capping mechanisms. It is believed that molecular capping agents play a significant role in the kinetic control of the nanocrystal growth by preferentially adsorbing to specific crystal faces, thus inhibiting growth of that surface. Probably the most commonly used chemical agents in the existing literature for the hydrothermal synthesis of ZnO NRs are $Zn(NO_3)_2$ and hexamethylenetetramine (HMT) (Boyle et al., 2002; Vayssieres, 2003; Tak & Yong, 2005; Song & Lim, 2007). In this case, $Zn(NO_3)_2$ provides Zn^{2+} ions required for building up ZnO NRs. Using HMT as a structural director, Greene et al. (Greene et al., 2006)produced dense arrays of ZnO NRs in aqueous solution having controllable diameters of 30 – 100 nm and lengths of 2 – 5 μm. With addition of polyethylenimine (PEI) in the hydrothermal method, Qiu et al. able to synthesized well-aligned ZnO NRs arrays with a long length of more than 40 μm. However, without the additive PEI, the length of the NRs was not more than 5 μm. Guo et al. (Guo et al., 2011b) studied the factors influencing the size, morphology and orientation of the epitaxial ZnO NRs on the solution using hydrothermal method and discussed about tuning of the size and morphology.

The role of HMT in aqueous chemical method is still not clearly understood. HMT is a nonionic cyclic tertiary amine that can act as a Lewis base to metal ions and has been shown to be a bidentate ligand capable of bridging two zinc(II) ions in solution. In this case, HMT acts as a pH buffer by slowly decomposing to provide a gradual and controlled supply of ammonia, which can form ammonium hydroxide as well as complex zinc(II) to form $Zn(NH_3)_4^{2+}$ (Greene et al., 2006). Because dehydration of the zinc hydroxide intermediates controls the growth of ZnO, the slow release of hydroxide may have a profound effect on the kinetics of the reaction. Additionally, ligands such as HMT and ammonia can kinetically control species in solution by coordinating to zinc(II) and keeping the free zinc ion concentration low. HMT and ammonia can also coordinate to the ZnO crystal, hindering the growth of certain surfaces.

For the chemical growth of ZnO NRs, uniform distribution of ZnO nanocrystal seeds ware prepared on the Si substrate by thermal decomposition of a zinc acetate precursor. Then well–aligned ZnO NRs were synthesized by hydrolysis of zinc nitrate in water in the presence of HMT at 90°C. 25 mM equimolar concentration of zinc nitrate and HMT was used in the growth solution.

Figure 5 shows the well aligned ZnO NRs grown by aqueous chemical method with the help of ZnO seed layer. A high density ZnO NRs grew vertically on the substrate over a large area. The diameters of the NRs ranged from 30 to 40 nm and the length was about few

microns. As a characteristic, hexagonal facet of the ZnO NRs are clearly seen from the top view image.

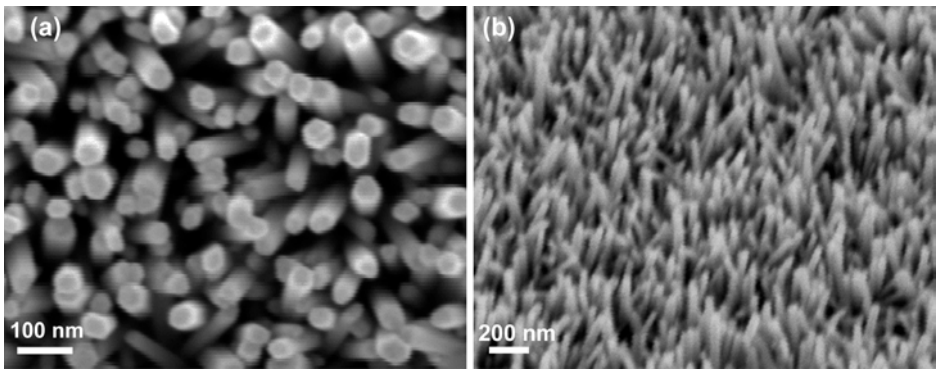

Fig. 5. FESEM images of ZnO nanorods grown on ZnO/Si substrate: (a) top view and (b) 45° tilted view.

3. Fabrication of ZnO nanorod heterostructures

It is considered that heterostructures are superior for the modulation of selective properties of that material. Using suitable external materials for the heterostructures, one can modify the properties of that material according to their requirements. In NRs structures, two types of heterostructures could be fabricated either longitudinal or radial/axial with suitable materials. Fabrication of planar semiconductor heterostructures for thin films is common, whereas the synthesis of one-dimensional heterostructures is difficult. Axial heterostructures, along the length of the NRs axis, have been reported for a few systems, such as InAs/InP, GaAs/GaP and Si/SiGe nanowires (Bjo¨rk et al., 2002; Gudiksen et al., 2002; Wu et al., 2002a). Recently there are reports on radial heterostructures of ZnO nanowires/NRs using several organic/inorganic materials (Bera & Basak, 2009a; Liu et al., 2010a; Bera & Basak, 2010; Liu et al., 2010b; Cheng et al., 2010a; Chang et al., 2011; Um et al., 2011). Bera et al. studied the radial heterostructure effect with poly(vinyl alcohol) on the photocarrier relaxation of the aqueous chemically grown ZnO nanowires. The photocurrent (PC) decay time during steady ultraviolet illumination has been reduced in the heterostructure, a decrease in the PC only by 12% of its maximum value under steady illumination for 15 min and a decrease in the PC by 49% of its maximum value during the same interval of time in the as-grown NWs. Three times enhancement in excitonic emission has been obtained by Liu et al. from the polymethyl methacrylate based ZnO NWs heterostructure. They explain this enhancement on the basis of surface states and energy band theory, due to the decrease in nonradiative process by surface modification. When ZnO NRs heterostructure was fabricated with another semiconducting material, ZnS, very high and faster photoconductivity and also enhanced UV PL intensity are obtained.

ZnO NRs covered with dense and uniform ultra small metal nanoparticles (NPs) is another form of heterostructures. Using suitable noble metal or low work function metal one could be able to achieve very high intense UV PL with significant reduction in visible emission, which is

one of the most important requirements for the application in UV LED or laser. Earlier, Lin et al. (Lin et al., 2006) and later Cheng et al. (Cheng et al., 2010b) reported on the significant enhancement of UV PL intensity and subsequent reduction in the defect related visible emission from the ZnO NRs covered with ultra small Au NPs. It is also observed that, after certain size of the Au NPs, the UV PL intensity start decreasing. They proposed that the obtained enhancement is due to the defect loss along with the localized surface Plasmon assisted recombination. Whereas when the NRs surface is covered with Ag NPs, a significant improvement in the yellow–green light emission is obtained (Lin et al., 2011). Interestingly, it is also observed that NRs covered with some metal gives rise to the decrement of the PL intensity (Fang et al., 2011). Although a significant changes is obtained from the metal NPs covered NRs, however a general mechanism for all types of metal covering is yet to emerge.

Here we fabricated ZnO NRs heterostructure by capping the surface with thin layer of anthracene (Dhara & Giri, unpublished). Anthracene/ZnO NRs heterostructures was fabricated by dip coating of the NRs in the diluted anthracene solution. We also fabricated another two heterostructure systems one with decoration of Au NPs and other with Ti NPs (Dhara & Giri, unpublished). From these heterostructures we investigated the origin of the enhanced photoconduction and photoluminescence. Metal NPs decoration was done by directly depositing NPs on the surface of the NRs by sputtering in a controlled way. For systematic study we decorated the surface with different sizes of the NPs by varying the sputtering time. Transmission electron microscope (TEM) image (Fig. 6) of the Au sputtered ZnO NRs shows uniform distribution Au NPs with sizes 3-6 nm coated over the surface of the NWs. The NRs grown by combined ZnO seed layer and Au catalyst using vapor transport method is used for heterostructure fabrication. Due to the vertical alignment of the NRs, Au NPs density is more at the top surface.

4. Structural and optical properties of the ZnO NRs

After the synthesis of nanostructures, it is essential to characterize the as-grown sample to know the structure and related properties. Low–dimensional nanostructures, with possible quantum–confinement effects and large surface area, show distinct mechanical, electronic and optical properties, compared to the bulk materials counterpart. In this section, we will summarise the structural characteristics of the ZnO NRs by x-ray diffraction (XRD), and TEM imaging, followed by optical properties, in particular optical absorption and emission.

4.1 Structural characterization

The structural characterization of the mechanosynthesized NRs was done by XRD shows (Fig. 7) characteristic peaks of pure hexagonal wurtzite phase of ZnO. It is observed that full width at half maximum (FWHM) of the XRD peaks increase monotonically with increase in reaction time. It is primarily due to the reduction of size of the NRs with increase in milling time. With increasing reaction time, the size of NRs decreases and strain is induced during the milling process, resulting in broadening of the XRD peaks.

Figure 8 (a) shows the low magnification TEM image of the 30 min reacted ZnO NRs. Length and diameter of the NRs for ZNR-0.5h sample varies in the range of 300-800 nm and 25-40 nm, respectively. With increase in reaction time, both diameter and length of the ZnO NRs are decreased due to mechanical milling process. During milling, the strain is developed; however, for prolonged milling when the strain is high, the crystal breaks up

and thus produces smaller sized NRs. After 5 h of milling, minimum diameter of ~15 nm is obtained (Fig. 8(b)). Fig. 8(b) also shows the high resolution lattice image of the NR with measured lattice spacing, 2.6 Å. The measured lattice spacing is in close agreement with the (002) plane of hexagonal structure. The selected area electron diffraction patterns (not shown) of the corresponding NR show the one–dimensional single–crystalline structures of the as-grown NRs.

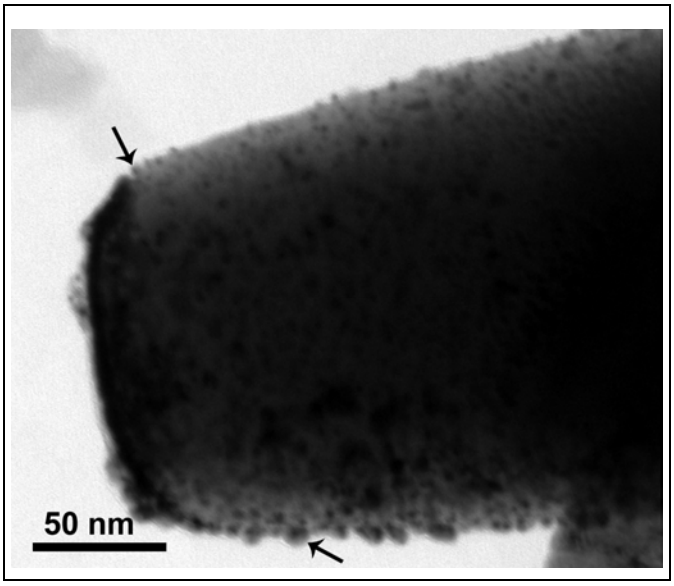

Fig. 6. TEM image of the Au NPs covered ZnO NRs, ultra small Au NPs on the surface of ZnO NRs are shown by solid arrows.

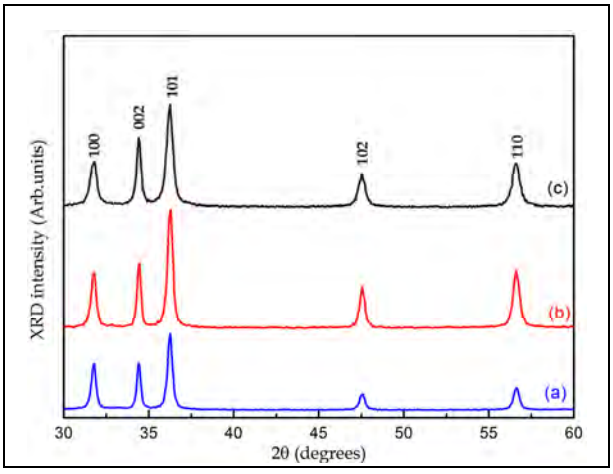

Fig. 7. XRD patterns of the mechanosynthesized ZnO NRs with reaction time: (a) 30 min, (b) 2 h, and (c) 5 h.

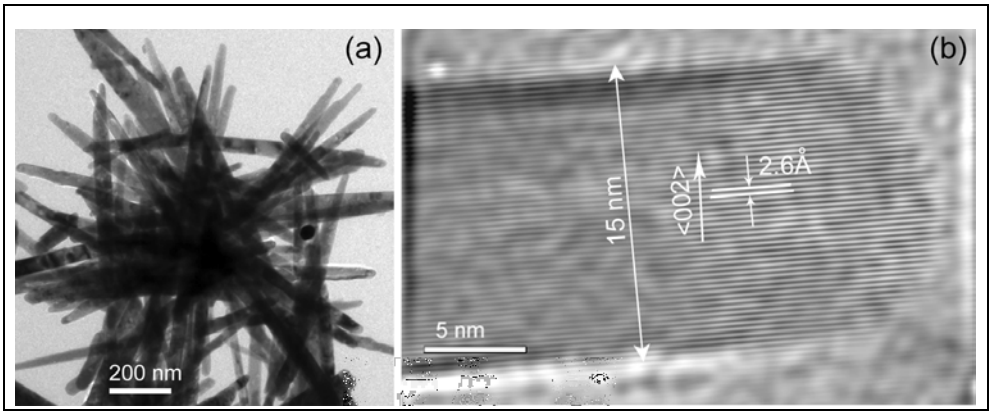

Fig. 8. TEM images of the mechanosynthesized ZnO NRs with reaction time; (a) 2 h, and (b) high–resolution lattice image of the 5h sample.

Figure 9 shows the XRD patterns of the ZnO NRs grown on Au coated ZnO seed layer at 900, 850 and 700°C respectively. The observed patterns shows only one strong diffraction peak indicates very high crystallinity. One strong (002) peak of hexagonal ZnO indicates the c-axis orientation of the single crystalline ZnO NRs, which are well aligned and the growth direction is perpendicular to the base surface. Relative intensities of the XRD peaks in Fig. 9 show that NRs grown at higher temperature have higher value of peak intensity, which confirms higher crystallinity. From XRD analysis, we have found that Au coating on ZnO seed layer induces a (111) orientation of the Au clusters at high temperature. Note that NRs grown without the seed layer does not show any preferred orientation and possess inferior crystallinity as compared to that grown with a seed layer. We have found that a substrate temperature below 800°C is not favourable for the growth of aligned NRs by VLS method.

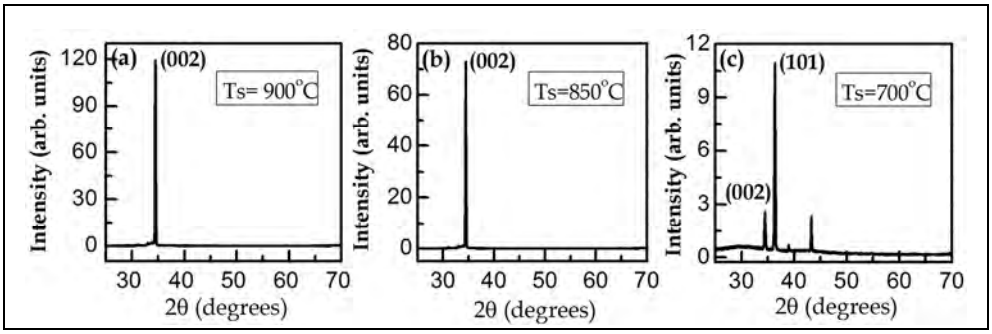

Fig. 9. XRD patterns of ZnO seed layer and Au catalyst assisted grown NRs array: grown at substrate temperature (a) 900, (b) 850 and (c) 700°C, respectively

4.2 Optical properties

As the energy band structure and bandgap reflects on the optical properties of the semiconductors, optical absorption spectroscopy is one of the important tool to probe the

energy bandgap. UV-Vis absorption spectra of all the mechanosynthesis samples are shown in Fig. 10. Observed peaks in the UV region correspond to the excitonic absorption of ZnO. A clear blueshift in the absorption peak is observed from 369 nm to 365 nm, as the size reduces from 40 nm to 15 nm. The observed blueshift is indicative of the increase in bandgap with decrease in size of the NRs. This blueshift with size reduction cannot be attributed fully to quantum size effect in ZnO NRs as these NRs have diameters in the range 15-40 nm, which is much higher than excitonic-Bohr diameter in ZnO (~6.48 nm). Therefore, the change in bandgap is partly contributed by the strain induced band–widening. Rapid thermal annealing (RTA) is an effective and simple tool to reduce the strain as well as to improve structural quality. After RTA, a redshift in the excitonic absorption is observed from all the samples, with respect to as-synthesized sample. This redshift is an indication of the decrease in band gap energy as the result of recrystallization and strain relaxation of the NRs (Chakraborty et al., 2011).

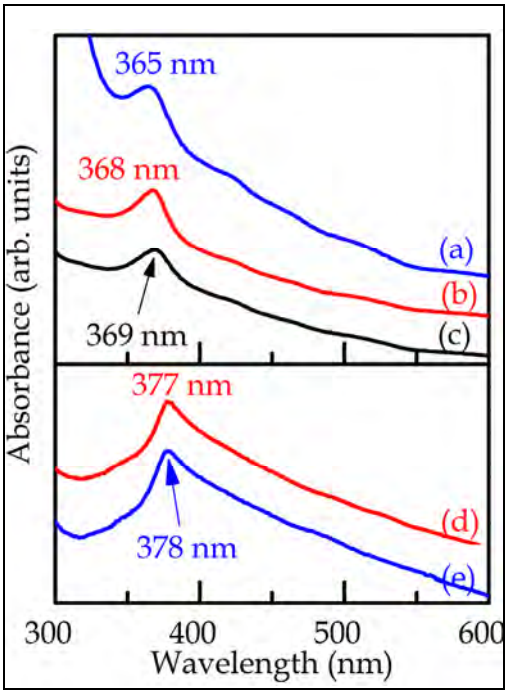

Fig. 10. UV–visible absorption spectra of (a) 5 h, (b) 2 h, and (c) 30 min mechanosynthesized ZnO NRs. Effect of RTA at (d) 500°C and (e) 700°C on the 2 h samples.

The room temperature PL spectra of the mechanosynthesized NRs show three distinct peaks (I-III) in the UV–blue region and one strong broad peak (IV) in the visible region. From 30 min to 5 h samples a blueshift in peak I is observed from 379 to 374 nm. This UV emission is due to the bound excitonic recombination. The peak II at ~390 nm is likely to be due to band-to-band transition between band tail states (Wang et al., 2002a). These band tail states are primarily caused by the presence of defects at the surface of the NRs. The peak III at

~409 nm is caused by the presence of zinc vacancy related defect states. The visible peak (IV) at 582 nm is very broad and it is likely to be related to the atomic disorder at the surface of the NRs caused by milling-induced lattice strain (Giri et al., 2007). An elegant review on presence of various defects in ZnO and corresponding emissions is presented by McCluskey et al. (McCluskey & Jokela, 2009). RTA-treated NRs show reduction in intensity of the peak IV as a result of strain relaxation, whereas intensity of the other three peaks is significantly enhanced. Interestingly, after RTA treatment, peaks II and III are shifted to higher wavelengths. The lattice strain may change the position of the intermediate defect-related states in the band structure of ZnO NRs. Recrystallization of NRs during RTA process is responsible for the change in the band gap and corresponding redshift in the PL spectra.

Figure 12 is corresponding to the PL spectra of the as-grown NRs grown at 900, 850, 700°C, respectively. VLS grown NRs shows two peaks in the PL spectra, one at UV region and other one at green region. The first one is the near band edge (NBE) related excitonic emission and latter one is the oxygen vacancy related defect emission, so called green emission band. The intensity of the UV PL gradually increases with the decrease in growth temperature. The lower intensity of NBE emission from vertically aligned NRs is primarily due to the lower area of absorption by the tip of the aligned NRs and corresponding emission. It is also possible that at higher temperature presence of oxygen vapour is relatively low compared to the low temperature region, which results in the formation of large no of oxygen vacancy states in the ZnO NRs. As a result strong green emission is observed from the NRs grown at higher temperature

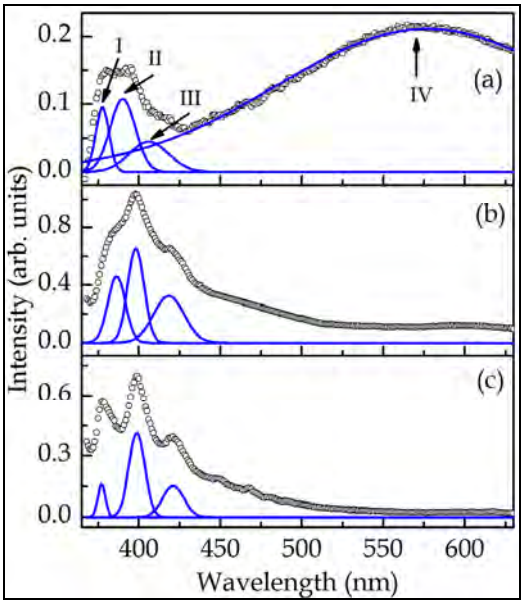

Fig. 11. PL spectra of 2 h mechanosynthesized ZnO NRs (a), after RTA at 500°C (b) and 700°C (c), respectively. Four peaks are fitted with Gaussian function (solid line) to the exp. data (symbol).

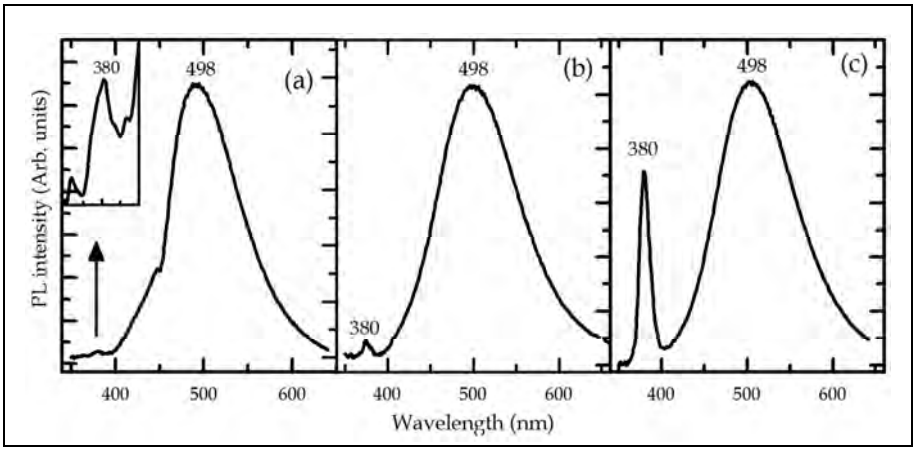

Fig. 12. PL spectra of combined seeded layer and Au catalyst grown aligned ZnO NRs at various substrate temperatures: (a) 900°C, (b) 850°C, (c) 700°C.

5. Photodetection behaviours of the ZnO NRs

Electronic conductivity of the ZnO NRs significantly enhanced when it is exposed to the light with wavelength below 380 nm. Using this property, ZnO NRs can be used for UV photodetectors. The dramatic change of conductance between dark and UV exposure suggest that the ZnO NRs photodetectors are also good candidates for optoelectronic switches, with the dark state as "OFF" and the UV exposed state as "ON". In the step towards the efficient and faster photodetection from ZnO NRs/nanowires some important works have been done recently, which are summarize in Table 1. Several types of approaches have been reported e.g. structural improvement, efficient doping, and heterostructures formation with suitable external materials. Zhou et al. (Zhou et al., 2009) used nonsymmetrical Schottky-type (ST) contact devices and obtained higher sensitivity and faster reset time. Pt microelectrode arrays were first fabricated on a SiO_2 /Si substrate by UV lithography to make Schottky–type contact on one end of the nanowires and a focused-ion-beam (FIB) deposited Pt-Ga electrode on other end of the ZnO nanowire for a good Ohmic contact. He and coauthors utilized FIB technique to deposit Pt metal on ZnO nanowires to effectively reduce the contact resistance, and thus achieved high photoconductive gain as high as 10^8. Chang et al. report the synthesis of a ZnO NR/graphene heterostructure by a facile *in situ* solution growth method (Chang et al., 2011). By combining the attributes of photosensitive ZnO NRs and highly conductive graphene, they are able to fabricate a highly sensitive visible-blind ultra UV sensor. Recently, Park and coauthors obtained enhanced photoresponse from isopropyl alcohol treated ZnO nanowire devices by introducing surface roughness induced traps (Park et al., 2011). They propose that obtained enhancement is attributed to an increase in adsorbed oxygen on roughening induced surface traps.

Therefore it is very important to have detail understanding about current conduction mechanism and origin of enhancement from the heterostructures. It should be mentioned that, till now, the lack of well-established fabrication method and standard procedures make it difficult to compare the experimental results between different devices.

Morphology	Device Type	Light of Detection (nm)	Bias (V)	Maximum Photosensitivity	Photosensitivity enhancement factor from unmodified photodetector	Reference
Nanowire	Resistor	365	5	10^4-10^6	–	(Kind et al., 2002)
Nanorods	Resistor	325	2	19	–	(Ahn et al., 2004)
Nanowires film	Resistor	254	5	17.7	–	(Li et al., 2005)
Nanorod	FET	254	0.2	1000	–	(Park et al., 2005)
Nanowire	Resistor	390	5	10^4	–	(Soci et al., 2007)
Nanowires arrays	Resistor	325	3	18000	~2.6	(Bera & Basak, 2009a)
Nanowires arrays	Resistor	360	3	10^4	~2.8	(Bera & Basak, 2009b)
Nanowire	Resistor	365	1	1500	~4	(Zhou et al., 2009)
Nanowire	Resistor	254	4	1800	~9.4	(Lin et al., 2009)
Nanowires arrays	Resistor	370	3	3367	`~5.2	(Bera & Basak, 2010)
Nanowires film	Resistor	365	8	–	~4.7	(Liu et al., 2010a)
Nanorods	Resistor	360	10	80	–	(Manekkathodi et al., 2010)
Nanowires arrays	Resistor	369	2.5	24200	~5.4	(Dhara & Giri, 2011a)
Nanorod	Resistor	370	20	–	~3.0	(Chang et al., 2011)
Nanowires	*n-i-n* junction	365	-5	1345	–	(Kim et al., 2011a)
Nanorods (interdigitated)	Resistor	379	5	12.1mA/W	–	(Guo et al., 2011a)
Nanowires arrays	Resistor	360	5	7600	~2.2	(Bera & Basak, 2011)
Nanowire	FET	365	0.4	10^6	~1.8	(Park et al., 2011)
NWs network	Resistor	254	5	52	~3	(Kim et al., 2011b)

Table 1. The performance characteristics of ZnO NRs/nanowires based photodetectors reported in the literature.

5.1 Dark I–V characteristics

Recently we have shown that presences of native surface defects (oxygen vacancies) could be identified from the dark I–V curves (Dhara & Giri, 2011a). The charge-depletion layer induced by surface adsorption of oxygen molecules completely controls the charge transport in NRs, if the diameter of the NRs is comparable to the depletion layer thickness. Another important step in determination of the electrical properties of NRs is the metal–NRs interface through metal electrode. In addition to the above factors, in case of nanowires network structures, charge transport is also determined by the nanowire– nanowire

contacts. The dark current-voltage (I-V) characteristic of the as-grown NRs shown in Fig. 13 shows a linear behavior up to a certain bias voltage. A linear fit to log-log plot of the I–V data could give detailed information about the mechanism of current conduction process. There is a crossover point of linear fitting around at 8V. Below this bias voltage, the power dependence of current on voltage is exactly 1, indicating an Ohmic conduction region, beyond which the current dependence on voltage is greater than one. This is most likely to be space charge limited current (SCLC) (Rose, 1955; Ohkubo et al., 2008), which arise from charge carriers trapped at the surface defect states that contribute to the current at higher bias voltage. In case of SCLC, power dependence greater than two could be observed depending on the energy distribution of trap centers. As the RTA treated NRs have very less native defects due to structural improvement and release of built in stress, a linear curve is expected. The NRs RTA treated at 800°C shows exactly a linear behavior, as expected.

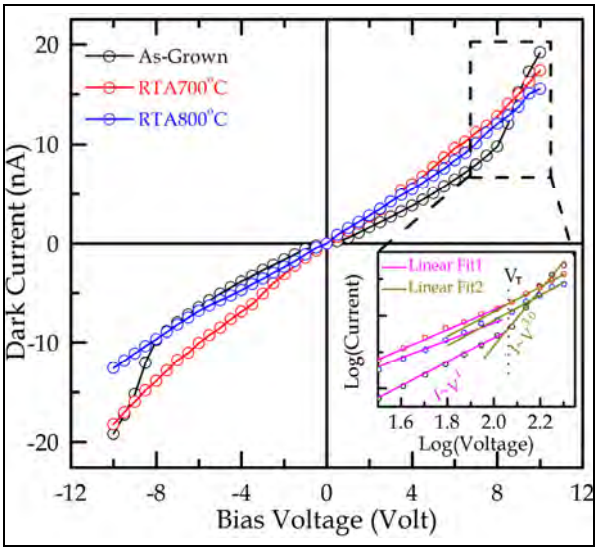

Fig. 13. The dark current-voltage characteristics of as-grown and RTA-treated ZnO NWs processed at 700°C and 800°C. Inset shows the magnified view of the selected region in log-log scale.

5.2 Spectral dependence of photodetection

Wavelength dependent PC studies of the ZnO NRs shows that it gives very high PC when it is exposed to the UV light (Fig. 14). The maximum PC is obtained at the excitation of 369 nm light, which is the band gap wavelength of ZnO NRs. The observed strong peak at 369 nm in the PC spectra is due to the band-edge absorption followed by generation of photocarriers (electron-hole pair). The small hump–like peaks in the visible region are due to the generation of carriers from the native defect states. In this case, the photosensitivity (photo-to-dark current ratio) is ~4500, which is quite low. By structural improvement or heterostructure formation, above hump could be eliminated and a visible–blind ZnO NRs based photodetectors with high sensitivity could be made.

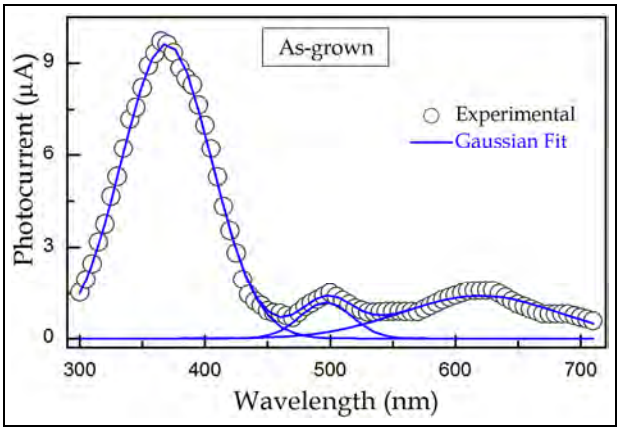

Fig. 14. The photocurrent spectra of the ZnO NRs measured at 2.5 V bias.

5.3 Photoresponse

The photoresponse behaviour of the ZnO NRs measured under the excitation of 365 nm UV light is shown in Fig. 15. It is seen that PC initially grows very fast and then slowly increased with time and finally saturated (mechanism is explain in next sub-section). The time-dependent PC growth and decay curves are fitted with the following equation (Dhara & Giri, 2011a),

$$I_{ph}(t) = I + A_1(1 - e^{-t/\tau_1}) - A_2 e^{-t/\tau_2} \quad (1)$$

$$I_{ph}(t) = I_{ph}(\infty) + A_3 e^{-t/\tau_3} + A_4 e^{-t/\tau_4} \quad (2)$$

where I, A_1, A_2, A_3 and A_4 are positive constants and $I_{ph}(\infty)$ refers to the photocurrent after infinitely long time of the decay experiment, which essentially is the dark current. The first exponential term in the growth and decay equations corresponds to the electron-hole generation and recombination processes and the last exponential term represents the oxygen adsorption process. Calculated time constants from fittings are τ_1 = 25.7 s and τ_2 = 347.9 s for PC growth, τ_3 =19.3 and τ_4 =316.0 s for PC decay, respectively. The photoresponse time for the as-grown NRs is very slow due to the presence of intrinsic defects/trap centres.

5.4 Photodetection mechanism of ZnO NRs

It is known that, the photoresponse of the ZnO NRs consists of two parts: a rapid process of photogeneration and recombination of electron–hole pairs, and a slow process of surface adsorption and photodesorption of oxygen molecules (Dhara & Giri, 2011a). The oxygen plays a crucial role in the photoresponse of ZnO. In dark condition, oxygen molecules from the air are easily stuck on the NRs surface by adsorption process and trapped electrons [$O_2(g)+e^- \rightarrow O_2^-$] available on the surface near the Zn lattice and decreased the conductivity (Kind et al., 2002), which is shown schematically in Fig. 16(a). This process leads to the formation of depletion layer near the surface resulting in the band bending of the conduction band (C.B) and the valence band (V.B). Formation of large number of ionized

oxygen on the NWs surface enhances the band bending, resulting in a very low conductivity. During the UV illumination, electron-hole pairs are generated [$h\nu \rightarrow e^- + h^+$] by light absorption. Now these electrons/holes easily cross the depletion layers and contribute to the photoconduction process. At the same time, holes take part in the oxidization of ionized oxygen ($O_2^- + h^+ \rightarrow O_2(g)$, photodesorption process) and release one oxygen gas molecule by electron–hole recombination process (Fig. 16(b)). Then few of the released oxygen molecules are re-adsorbed on the surface and decrease the free electron carriers. The energy band diagram during UV illumination is shown in (c). After certain time electron-hole generation rate and oxygen re-adsorption rate becomes constant resulting in a steady photocurrent. It is known that adsorption process is slower than the photodesorption process. Therefore, during UV illumination, not all the holes are recombine with the electrons present in the ionized oxygen. As a result, excess holes are available for recombination with the exciton related free electrons. During photocurrent decay, the exciton related electron–hole recombination dominates, which corresponds to the faster decay component, so the photocurrent initially decreases very rapidly. With the surface re-adsorption of oxygen, the photocurrent comes to the initial value very slowly.

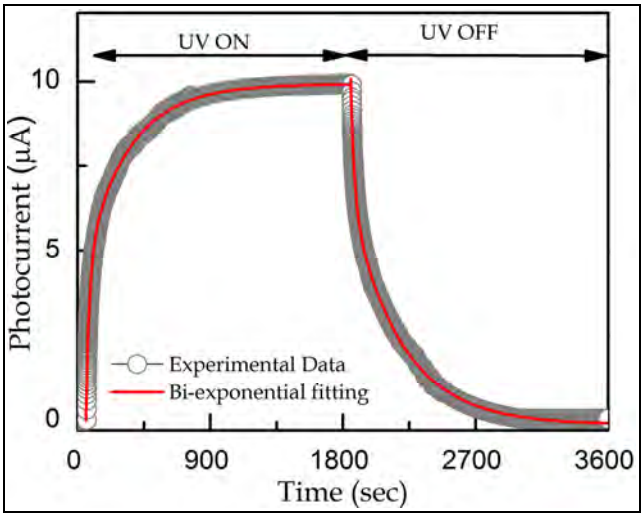

Fig. 15. The Photocurrent growth and decay behaviors (photoresponse) of as-grown ZnO NRs.

5.5 Effect of structural improvement

We have shown that a fivefold enhancement of photosensitivity in the UV region and faster photoresponse could be obtained from the ZnO NWs/NRs by structural improvement using RTA processing (Dhara & Giri, 2011a). The photocurrent growth and decay rates (photoresponse) from RTA-treated NWs are improved by a factor of approximately 2. After RTA at 800°C, the PC at 369 nm reaches a maximum value of 84.1 μA (Fig. 17) from that of 9.6 μA for the as-grown NWs, results in a sensitivity value of 24.2×10^3, leading to an enhancement factor of five. The PC growth and decay time constants are improved to 12.3 and 107.0 s for growth, 13.6 and 118.4 s for decay. The RTA processing substantially

removes the surface defect-related trap centers and modified the surface of the ZnO NWs, resulting in enhanced PC and faster photoresponse. During RTA processing, the NRs recrystallize and structural quality is improved by releasing built-in stress and removing the defect states. Due to reduction of surface defects, the PC in the visible region drastically decreased. Therefore RTA processed photodetector is fully visible–blind and only sense the UV light. The high photosensitivity even in low light intensity is an indication of very low value of detection limit.

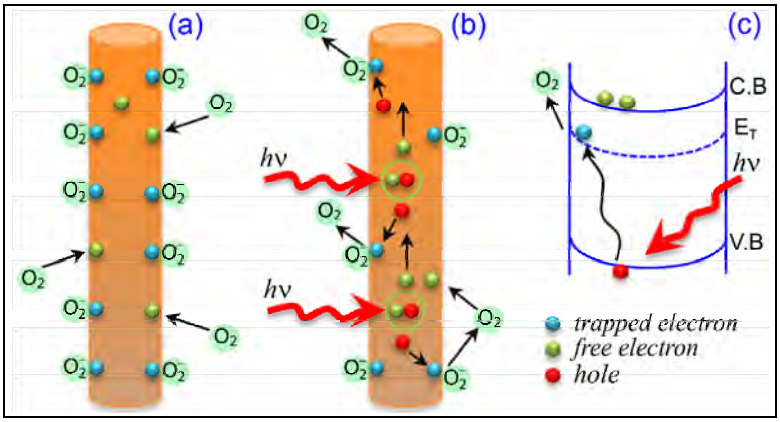

Fig. 16. A schematic of photoresponse mechanism of ZnO NRs: (a) at dark condition and (b) during UV illumination. (c) Schematic energy band diagram of photoresponse process during UV illumination.

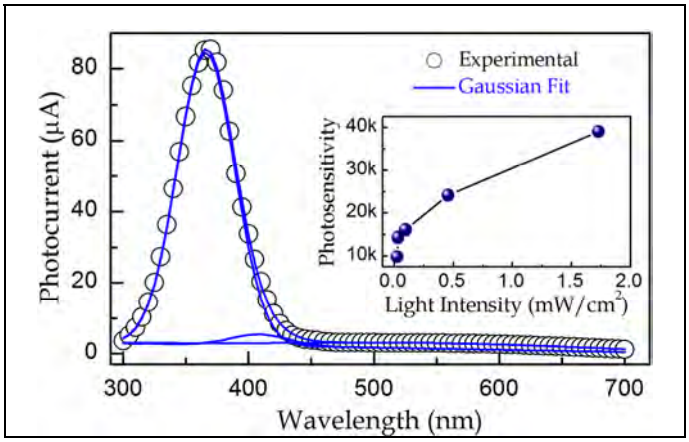

Fig. 17. The photocurrent spectra of the ZnO NRs after RTA treated at 800°C.

5.6 Effect of heterostructure by surface capping

Here we present the effect of surface capping on the ZnO NRs with anthracene on the enhancement of PC and photoresponse. Although the dark current is almost doubled after

the capping, however a significant improvement in the photosensitivity is obtained. Compared to the as-grown case, the photoresponse time becomes much faster for the ZnO/anthracene system with response and reset times within second (Dhara & Giri, unpublished). The reasons for choosing anthracene are that it can act as UV sensitive material to enhance the photosensitivity and it can influence the oxygen adsorption process. After anthracene capping the maximum photocurrent increases to 50 μA from 4 μA, which is for as–grown NRs (Fig. 18). Photosensitivity value is also increased to 4183, leading to the six–fold enhancement. Very high photosensitivity and low dark current are the basic requirements for efficient photodetection. Due the surface capping, the surface of the NRs becomes modified and in this case thickness of the depletion layer is much lower than the case of as–grown NRs. When the sizes of the nanostructures are comparable to the space charge layer, surface depletion greatly affects the density and the mobility of the carriers in ZnO NWs rather than the contact potential (Li et al., 2007). Here anthracene layer is very thin and the carriers easily tunnel through the layer to the electrodes, resulting in increment in dark current.

The photoresponse spectrum (Fig. 19) measured at 360 nm shows very fast response with response and reset times of 1.5 and 1.6 s, respectively (the response and reset time can be defined as 1-1/e, (63%) of the maximum photocurrent increased and 1/e, (37%) of the maximum photocurrent decreased, respectively). In contrast, the as-grown NRs have response and reset time about 7.2 and 63.2 s, respectively. Therefore anthracene capped ZnO NRs heterostructure has five times faster response time and about forty times faster reset time, which is very good for real time application. Here, the anthracene has strong absorption in the UV region, when it is excited with UV light the photoexcited charge carriers transfer to the conduction band of ZnO NRs. This process results in high photocurrent and consequent higher photosensitivity. Modification/reduction of surface defects related traps by anthracene capping is also responsible for the obtained very high photocurrent.

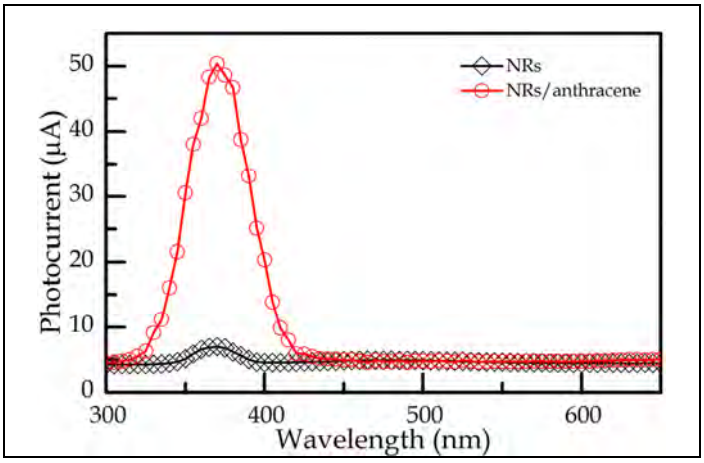

Fig. 18. Photocurrent spectra of the as-grown ZnO NRs and ZnO/anthracene based NRs heterostructure.

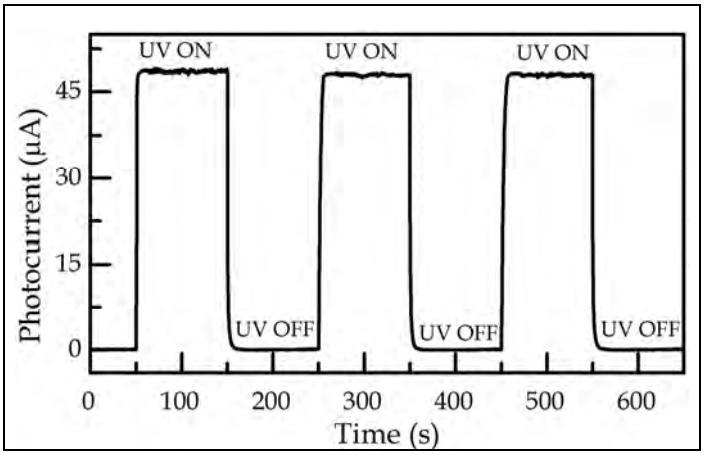

Fig. 19. Photoresponse behavior (at 360 nm) of the ZnO/anthracene based NRs heterostructure in a repetitive UV light "ON" and "OFF" conditions.

5.7 Metal NPs decorated ZnO NRs heterostructures

In case of Au/ZnO heterostructures, Au NPs and ZnO NRs interface actively interplay on the photodetection process. Au/ZnO heterostructure shows nearly linear dark I–V characteristic with reduced dark current. The decrement of current is more prominent in the lower bias voltage and at higher bias voltage it reached very close to the dark current of as-grown NWs. It is known that when a metal is brought in contact with semiconductor, it induces band bending due to the equilibrium of Fermi level (Liao et al., 2007; Dayeh et al., 2007). Depending on the difference in the work–functions of metal and semiconductor, two types of contacts have been formed at the metal semiconductor interface. Therefore, the decrement in dark current is due to the large upward band bending and formation of Schottky barrier at the interface between Au and ZnO. Because, Au has larger work–function, 5.47 eV (Lide, 2009) than ZnO, 4.65 eV (Aguilar et al., 2009). As a result, no electron will be transfer from Au to the conduction band of ZnO. However, at a lower bias voltage few numbers of electrons can pass from ZnO to the Al electrode, giving very low dark current. At higher bias voltage, which is greater than the Schottky barrier height, all the electrons can flow to external circuit giving almost equal dark current as for the case of as-grown NRs.

As expected, the as-grown NRs shows low PC in the UV region (Fig. 20.), whereas it is significantly enhanced after Au NPs decoration. Here seven times enhancement in the photosensitivity is obtained. The broad photocurrent peak from the Au/ZnO heterostructures in the visible region is due to the Au NPs absorption related carrier transfer to the conduction band of ZnO. As the dark current of the Au/ZnO heterostructures is lower than the as-grown ZnO NRs, a lower PC is expected. However, the obtained PC is quite high. In this case, with respect to the vacuum level, the energy level of oxygen vacancy defect states (5.43 eV) and Fermi level of Au (5.47 eV) is very close to each other (Lide, 2009). Therefore, the electrons from this defect states can transfer to the Fermi level of Au, which increases the electron density at the Fermi level of Au. The Au NPs are excited by incident light in the UV-violet

region due to interband transition and in the green region due to the surface Plasmon resonance (SP band) (Garcia, 2011). After that the excited energetic electrons are stay in higher energy states, and these are so active that they can escape from the surface of the NPs and can transfer to the conduction band of ZnO. Under bias, these electrons along with electrons generated by band edge absorption of ZnO contributed to the current conduction process. Therefore, the obtained enhanced photocurrent in the UV as well as in the visible region is due to the increase of electron density in the conduction band of ZnO by ZnO band edge absorption and electron transport via Au NPs (Dhara & Giri, unpublished).

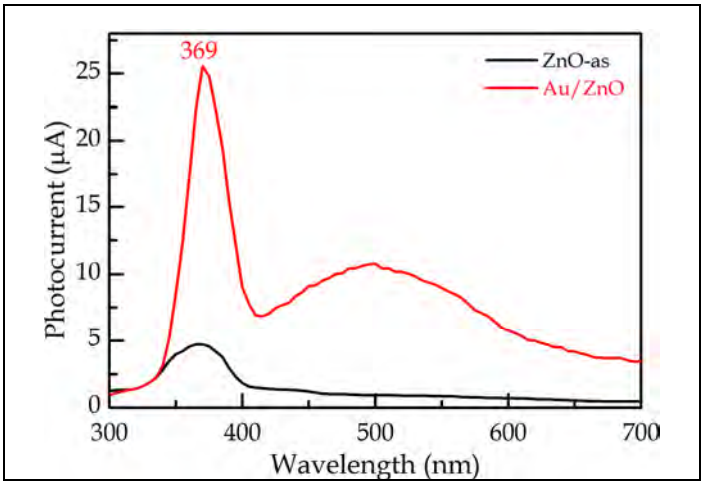

Fig. 20. Photocurrent spectra of the as–grown NRs and Au NPs decorated Au/ZnO NRs heterostructures.

A faster photoresponse is obtained from the Au/ZnO heterostructures and it is almost independent of the thickness of the Au layer. The response and reset times are as fast as 26.5 s and 70.0 s. In this case due to the decoration of Au NPs, surface of the ZnO NWs becomes modified and facilitated to increase the adsorption and desorption process, resulting in faster photoresponse.

On the contrary, Ti NPs decorated heterostructures show a linear I–V behavior with very high dark current. The dark current gradually increases with increase in Ti coverage. Due to the lower work–function of Ti (4.26 eV) (Lide, 2009) compared to ZnO, an Ohmic contact is formed with downward band bending. In this case, more numbers of electrons can easily transfer from Ti to the conduction band of ZnO at the interface. Then under the bias these electrons contributes to the current conduction process results in high dark current.

The PC in the UV region is drastically enhanced at an excitation wavelength of 369 nm. The Ti/ZnO heterostructure gives PC of 65.5 μA. Although the obtained PC from Ti/ZnO heterostructure is very high, but due to higher dark current the photosensitivity values are low. The photoresponse behaviours of the Ti decorated ZnO NRs show very fast response with response and reset time within few seconds. The fastest response time of 5.5 s and reset time of 7.7 s is obtained. These data indicate a significant improvement in the photoresponse

process and much faster photoresponse could be obtained from Au or Ti decorated ZnO NRs heterostructures.

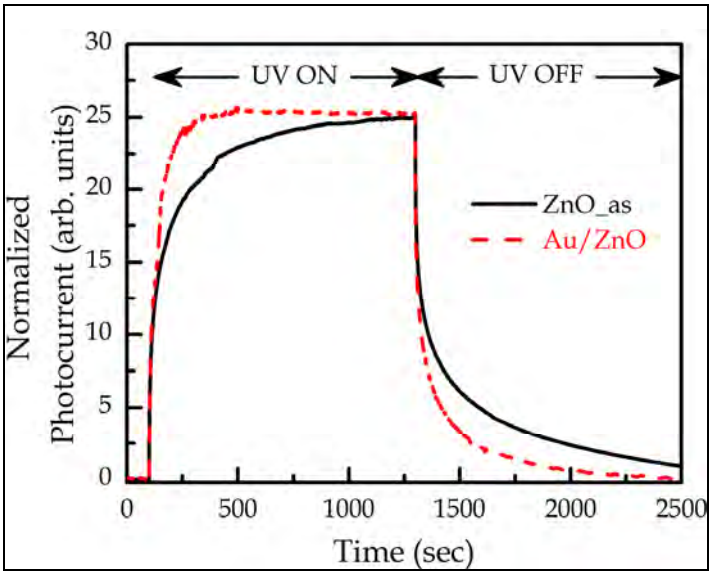

Fig. 21. Photoresponse behaviours of the as-grown NRs and Au NPs decorated Au/ZnO NRs heterostructures under the illumination of 365 nm UV light.

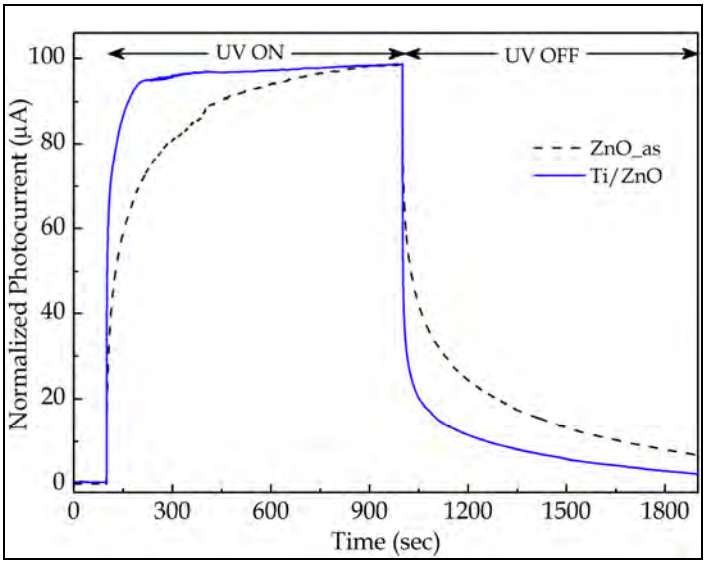

Fig. 22. Photoresponse behaviours of the as-grown NRs and Ti NPs decorated Ti/ZnO NRs heterostructure under the illumination of 365 nm UV light.

6. Summary

Here we reviewed our recent achievement on the controlled growth of vertically aligned ZnO NRs arrays and their heterostructures for the applications of efficient UV photodetection. We provided a summary of effects of several growth parameters on different growth methods for the well aligned ZnO NRs arrays. ZnO NRs arrays grown by three different methods; mechanosynthesis, vapour–liquid–solid and aqueous chemical methods are presented here. It is shown that the combined effects of ZnO seed layer and Au catalyst are favourable for the growth of well aligned ZnO NRs arrays. Three different types of ZnO NRs based heterostructures were fabricated; one with surface capping of anthracene and others with surface decoration of Au and Ti NPs with suitable sizes. Photodetection behaviours of the different systems are studied by dark I–V characteristics, wavelength dependent photocurrent and photoresponse. The results demonstrate that ZnO NRs heterostructures are indeed excellent candidates for UV photodetectors with very high sensitivity and faster response for real time sensing applications. Possible mechanisms of improved photodetection behaviours from different systems are also presented. These understanding will help to design and fabricate a ZnO NRs heterostructure based efficient UV photodetectors. An up–to–date summary of important results by several research groups worldwide on the ZnO NRs/NWs heterostructures based UV photodetectors is presented in Table 1. Our approaches show comparable significant improvement over several reports on ZnO NRs based photodetectors.

7. References

Aguilar, C. A.; Haight, R.; Mavrokefalos, A.; Korgel, B. A. & Chen, S. (2009). Probing electronic properties of molecular engineered zinc oxide nanowires with photoelectron spectroscopy. *ACS. Nano*, Vol.3, pp. 3057–3062

Ahn, S. E.; Lee, J. S.; Kim, H.; Kim, S.; Kang, B. K.; Kim, K. H. & Kim, G. T. (2004). Photoresponse of sol-gel-synthesized ZnO nanorods. *Appl. Phys. Lett.*, Vol.84, pp. 5022–5024

Alvi, N. H.; Riaz, M.; Tzamalis, G.; Nur, O. & Willander, M. (2010). Fabrication and characterization of high-brightness light emitting diodes based on n-ZnO nanorods grown by a low-temperature chemical method on p-4H-SiC and p-GaN. *Semicond. Sci. Technol.*, Vol.25, pp. 065004

Ao, W.; Li, J.; Yang, H.; Zeng, X. & Ma, X. (2006). Mechanochemical synthesis of zinc oxide nanocrystalline. *Powder Technol.*, Vol.168, pp. 148-151

Bera, A. & Basak, D. (2009a). Effect of surface capping with poly(vinyl alcohol) on the photocarrier relaxation of ZnO nanowires. *ACS Appl. Mater. Interface*, Vol.1, pp. 2066–2070

Bera, A. & Basak, D. (2009b). Role of defects in the anomalous photoconductivity in ZnO nanowires. *Appl. Phys. Lett.*, Vol.94, pp. 163119

Bera, A. & Basak, D. (2010). Photoluminescence and Photoconductivity of ZnS-Coated ZnO Nanowires. *ACS. Appl. Mater. Interfaces*, Vol.2, pp. 408–412

Bera, A. & Basak, D. (2011). Pd-nanoparticle-decorated ZnO nanowires: ultraviolet photosensitivity and photoluminescence properties. *Nanotechnol.* , Vol.22, pp. 265501

Bjo¨rk, M. T.; Ohlsson, B. J.; Sass, T.; Persson, A. I.; Thelander, C.; Magnusson, M. H.; Deppert, K.; Wallenberg, L. R. & Samuelson, L. (2002). One-dimensional heterostructures in semiconductor nanowhiskers. *Appl. Phys. Lett.*, Vol.80, pp. 1058-1060

Boyle, D. S.; Govender, K. & O'Brien, P. (2002). Novel low temperature solution deposition of perpendicularly orientated rods of ZnO: Substrate effects and evidence of the importance of counter-ions in the control of crystallite growth. *Chem. Commun.*, pp. 80–81

Breedon, M.; Rix, C. & Kalantar-zadeh, K. (2009). Seeded growth of ZnO nanorods from NaOH solutions. *Mater. Lett.*, Vol.63, pp. 249–251

Chakraborty, R.; Dhara, S. & Giri, P. K. (2011). Effect of rapid thermal annealing on microstructure and optical properties of ZnO nanorods. *Int. J. Nanosci.*, Vol.10, pp. 65-68

Chang, H.; Sun, Z.; Ho, K. Y.; Tao, X.; Yan, F.; Kwok, W. M. & Zheng, Z. (2011). A highly sensitive ultraviolet sensor based on a facile in situ solution-grown ZnO nanorod/graphene heterostructure. *Nanoscale*, Vol.3, pp. 258–264

Chen, C. C.; Yeh, C. C.; Chen, C. H.; MY, M. Y. Y. & Liu, H. L. (2001). Catalytic growth and characterization of gallium nitride nanowires. *J. Am. Chem. Soc.*, Vol.123, pp. 2791-2798

Chen, L.-Y.; Wu, S.-H. & Yin, Y.-T. (2009). Catalyst-free growth of vertical alignment ZnO nanowire arrays by a two-stage process. *J. Phys. Chem. C*, Vol.113, pp. 21572-21576

Cheng, C.; Wang, T.-L.; Feng, L.; Li, W.; Ho, K. M.; Loy, M. M. T.; Fung, K. K. & Wang, N. (2010a). Vertically aligned ZnO/amorphous-Si core-shell heterostructured nanowire arrays. *Nanotechnol.*, Vol.21, pp. 475703

Cheng, C. W.; Sie, E. J.; Liu, B.; Huan, C. H. A.; Sum, T. C.; Sun, H. D. & Fan, H. J. (2010b). Surface plasmon enhanced band edge luminescence of ZnO nanorods by capping Au nanoparticles. *Appl. Phys. Lett.*, Vol.96, pp. 071107

Cui, J. B.; Daghlian, C. P.; Gibson, U. J.; Pusche, R.; Geithner, P. & Ley, L. (2005). Low-temperature growth and field emission of ZnO nanowire arrays. *J. Appl. Phys.*, Vol.97, pp. 44315

Dayeh, S. A.; Soci, C.; Yu, P. K. L.; Yu, E. T. & Wang, D. (2007). Influence of surface states on the extraction of transport parameters from InAs nanowire field effect transistors. *Appl. Phys. Lett.*, Vol.90, pp. 162112

Dhara, S. & Giri, P. K. (2011a). Enhanced UV photosensitivity from rapid thermal annealed vertically aligned ZnO nanowires. *Nanoscale Res. Lett.*, Vol.6, pp. 504

Dhara, S. & Giri, P. K. (2011b). Quick single-step mechanosynthesis of ZnO nanorods and their optical characterization: milling time dependence. *Appl. NanoSci*, Vol.1, pp. 165-171, doi:10.1007/s13204-011-0026-z

Dhara, S. & Giri, P. K. (2011c). Shape evolution in one-dimensional ZnO nanostructure grown from ZnO nanopowder source: vapour-liquid-solid vs. vapour-solid growth mechanisms. *Int. J. Nanosci.*, Vol.10, pp. 75-79

Dhara, S. & Giri, P. K. (unpublished).

Ding, J.; Miao, W. F.; McCormick, P. G. & Street, R. (1995). Mechanochemical synthesis of ultrafine Fe powder. *Appl. Phys. Lett.* , Vol.67, pp. 3804-3806

Duan, X. & Lieber, C. M. (2000). General synthesis of compound semiconductor nanowires. *Adv. Mater.*, Vol.12, pp. 298-302

Fang, Y. J.; Sha, J.; Wang, Z. L.; Wan, Y. T.; Xia, W. W. & Wang, Y. W. (2011). Behind the change of the photoluminescence property of metal-coated ZnO nanowire arrays. *Appl. Phys. Lett.*, Vol.98, pp. 033103

Feng, L.; Liu, A.; Liu, M.; Ma, Y.; Wei, J. & Man, B. (2010). Synthesis, characterization and optical properties of flower-like ZnO nanorods by non-catalytic thermal evaporation. *J. Alloys Comp.*, Vol.492, pp. 427-432

Gao, P. X.; Ding, Y. & Wang, Z. L. (2003). Crystallographic-orientation aligned ZnO nanorods grown by tin catalyst. *Nano Lett.*, Vol.3, pp. 1315-1320

Garcia, M. A. (2011). Surface plasmons in metallic nanoparticles: fundamentals and applications. *J. Phys. D: Appl. Phys.* , Vol.44, pp. 283001

Gargas, D. J.; Eugenia, M.; Molares, T. & Yang, P. (2009). Imaging single ZnO vertical nanowire laser cavities using UV-laser scanning confocal microscopy. *J. Am. Chem. Soc.*, Vol.131, No.6, pp. 2125-2127. doi:10.1021/ja8092339

Giri, P. K.; Bhattacharya, S.; Singh, D. K.; Kesavamoorthy, R.; Panigrahi, B. K. & Nair, K. G. M. (2007). Correlation between microstructure and optical properties of ZnO nanoparticles synthesized by ball milling. *J. Appl. Phys.*, Vol.102, pp. 093515

Giri, P. K.; Dhara, S. & Chakraborty, R. (2010). Effect of ZnO seed layer on the catalytic growth of vertically aligned ZnO nanorod arrays. *Mater. Chem. Phys.*, Vol.122, pp. 18-22

Givargizov, E. I. (1975). Fundamental aspects of VLS growth. *J. Cryst. Growth*, Vol.31, pp. 20-30

Greene, L. E.; Yuhas, B. D.; Law, M.; Zitoun, D. & Yang, P. (2006). Solution-Grown Zinc Oxide Nanowires. *Inorg. Chem.*, Vol.45, pp. 7535-7543

Gudiksen, M. S.; Lauhon, U. J.; Wang, J.; Smith, D. C. & Lieber, C. M. (2002). Growth of nanowire superlattice structures for nanoscale photonics and electronics. *Nature*, Vol.415, pp. 617–620

Gudiksen, M. S. & Lieber, C. M. (2000). Diameter-selective synthesis of semiconductor nanowires. *J. Am. Chem. Soc.*, Vol.122, pp. 8801-8802

Guo, L.; Zhang, H.; Zhao, D.; Yao, B.; Li, B.; Zhang, Z. & Shen, D. (2011a). The growth and the ultraviolet photoresponse properties of the horizontal growth ZnO nanorods *Mat. Lett.*, Vol.65, pp. 1495–1498

Guo, Z.; Andreazza-Vignolle, C.; Andreazza, P.; Sauvage, T.; Zhao, D. X.; Liu, Y. C.; B.Yao; Shen, D. Z. & Fan, X. W. (2011b). Tuning the growth of ZnO nanowires. *Physica B*, Vol.406, pp. 2200–2205

He, J. H.; Hsu, J. H.; Wang, C. W.; Lin, H. N.; Chen, L. J. & Wang, Z. L. (2006). Pattern and feature designed growth of ZnO nanowire arrays for vertical devices. *J. Phys. Chem. B*, Vol.110, pp. 50-53

Hejazi, S. R. & Hosseini, H. R. M. (2007). A diffusion-controlled kinetic model for growth of Au-catalyzed ZnO nanorods: Theory and experiment. *J. Cryst. Growth*, Vol.309, pp. 70–75

Heo, Y. W.; Varadarajan, V.; Kaufman, M.; Kim, K.; Norton, D. P.; Ren, F. & Fleming, P. H. (2002). Site-specific growth of ZnO nanorods using catalysis-driven molecular-beam epitaxy. *Appl. Phys. Lett.*, Vol.81, pp. 3046–3048

Huang, M. H.; Mao, S.; Feick, H.; Yan, H.; Wu, Y.; Kind, H.; Weber, E.; Russo, R. & Yang, P. (2001a). Room-temperature ultraviolet nanowire nanolasers. *Science*, Vol.292, pp. 1897-1899

Huang, M. H.; Wu, Y.; Feick, H.; Tran, N.; Weber, E. & P. Yang 13 (2001b). Catalytic growth of Zinc Oxidenanowires by vapor transport. *Adv. Mater.*, Vol.13, pp. 113-116

Kim, D. C.; Jung, B. O.; Lee, J. H.; Cho, H. K.; Lee, J. Y. & Lee, J. H. (2011a). Dramatically enhanced ultraviolet photosensing mechanism in a n-ZnO nanowires/i-MgO/n-Si structure with highly dense nanowires and ultrathin MgO layers. *Nanotechnol.*, Vol.22, pp. 265506

Kim, D. C.; Kong, B. H. & Cho, H. K. (2009). Synthesis and growth mechanism of catalyst free ZnO nanorods with enhanced aspect ratio by high flow additional carrier gas at low temperature. *J. Phys. D: Appl. Phys.*, Vol.42, pp. 065406

Kim, K.-P.; Chang, D.; Lim, S. K.; Lee, S.-K.; Lyu, H.-K. & Hwang, D.-K. (2011b). Effect of TiO2 Nanoparticle Modification on Ultraviolet Photodetection Properties of Al-Doped ZnO Nanowire Network. *J. J. Appl. Phys.*, Vol.50, pp. 06GF07

Kind, H.; Yan, H. Q.; Messer, B.; Law, M. & Yang, P. D. (2002). Nanowire ultraviolet photodetectors and optical switche. *Adv. Mater.*, Vol.14, pp. 158–160

Kirkham, M.; Wang, X.; Wang, Z. L. & Snyder, R. L. (2007). Solid Au nanoparticles as a catalyst for growing aligned ZnO nanowires: A new understanding of the vapour-liquid-solid process. *Nanotechnol.*, Vol.18, pp. 365304

Law, M.; Green, L. E.; Jhonson, J. C.; Saykally, R. & Yang, P. (2005). Nanowire dye-sensitized solar cells. *Nature Mater*, Vol.4, pp. 455-495

Law, M.; Greene, L. E.; Radenovic, A.; Kuykendall, T.; Liphardt, J. & Yang, P. (2006). ZnO-Al_2O_3 and ZnO-TiO_2 core-shell nanowire dye-sensitized solar cells. *J. Phys. Chem. B* Vol.110, pp. 22652-22663

Li, C.; Fang, G.; Li, J.; Ai, L.; Dong, B. & Zhao, X. (2008). Effect of seed layer on structural properties of ZnO nanorod arrays grown by vapor-phase transport. *J. Phys. Chem. C* Vol.112, pp. 990-995

Li, C.; Fang, G.; Su, F.; Li, G.; Wu, X. & Zhao, X. (2006). Synthesis and photoluminescence properties of vertically aligned ZnO nanorod–nanowall junction arrays on a ZnO-coated silicon substrate *Nanotechnol.*, Vol.17, pp. 3740

Li, C. C.; Du, Z. F.; Li, L. M.; Yu, H. C.; Wan, Q. & Wang, T. H. (2007). Surface-depletion controlled gas sensing of ZnO nanorods grown at room temperature. *Appl. Phys. Lett.*, Vol.91, pp. 032101

Li, Q. H.; Gao, T.; Wang, Y. G. & Wang, T. H. (2005). Adsorption and desorption of oxygen probed from ZnO nanowire films by photocurrent measurements. *Appl. Phys. Lett.*, Vol.86, pp. 123117

Li, S.; Zhang, X.; Yan, B. & Yu, T. (2009). Growth mechanism and diameter control of well-aligned small-diameter ZnO nanowire arrays synthesized by a catalyst-free thermal evaporation method. *Nanotechnol.*, Vol.20, pp. 495604

Li, S. Y.; Lee, C. Y. & Tseng, T. Y. (2003). Copper-catalyzed ZnO nanowires on silicon (100) grown by vapor–liquid–solid process. *J. Cryst. Growth* Vol.247, pp. 357-362

Liao, Z.-M.; Liu, K.-J.; Zhang, J.-M.; Xu, J. & Yu, D.-P. (2007). Effect of surface states on electron transport in individual ZnO nanowires. *Phys. Lett. A* Vol.367, pp. 207-210

Lide, D. R. (2009) CRC Handbook of Chemistry and Physics. CRC, Boca Raton

Lin, C.-A.; Tsai, D.-S.; Chen, C.-Y. & He, J.-H. (2011). Significant enhancement of yellow–green light emission of ZnO nanorod arrays using Ag island films. *Nanoscale*, Vol.3, pp. 1195-1199

Lin, D.; Wu, H.; Zhang, W.; Li, H. & Pan, W. (2009). Enhanced UV photoresponse from heterostructured Ag-ZnO nanowires. *Appl. Phys. Lett.* , Vol.94, pp. 172103

Lin, H. Y.; Cheng, C. L.; Chou, Y. Y.; Huang, L. L.; Chen, Y. F. & Tsen, K. T. (2006). Enhancement of band gap emission stimulated by defect loss. *Opt. Express*, Vol.16, pp. 2372-2379

Liu, J.; Ahn, Y. H.; Park, J.-Y.; Koh, K. H. & Lee, S. (2009). Hybrid light-emitting diodes based on flexible sheets of mass-produced ZnO nanowires. *Nanotechnol.*, Vol.20, pp. 4452063

Liu, J.; Park, J.; Park, K. H.; Ahn, Y.; Park, J. Y.; Koh, K. H. & Lee, S. (2010a). Enhanced photoconduction of free-standing ZnO nanowire films by L-lysine treatment. *Nanotechnol.*, Vol.21, pp. 485504

Liu, K. W.; Chen, R.; Xing, G. Z.; Wu, T. & Sun, H. D. (2010b). Photoluminescence characteristics of high quality ZnO nanowires and its enhancement by polymer covering. *Appl. Phys. Lett.*, Vol.96, pp. 023111

Lyu, S. C.; Zhang, Y. & Lee, C. J. (2003). Low-temperature growth of ZnO Nanowire array by a simple physical vapor-deposition method. *Chem. Mater.*, Vol.15, pp. 3294-3299

Lyu, S. C.; Zhang, Y.; Ruh, H.; Lee, H. J.; Shim, H. W.; Suh, E. K. & Lee, C. S. (2002). Low temperature growth and photoluminescence of well-aligned zinc oxide nanowires. *Chem. Phys. Lett.*, Vol.363, pp. 134-138

Mancheva, M.; Iordanova, R. & Dimitriev, Y. (2011). Mechanochemical synthesis of nanocrystalline $ZnWO_4$ at room temperature. *J. Alloys Comp.* , Vol.509, pp. 15-20

Manekkathodi, A.; Lu, M. Y.; Wang, C. W. & Chen, L. J. (2010). Direct growth of aligned zinc oxide nanorods on paper substrates for low-cost flexible electronics. *Adv. Mater.*, Vol.22, pp. 4059-4063

McCluskey, M. D. & Jokela, S. J. (2009). Defects in ZnO. *J. Appl. Phys.*, Vol.106, pp. 071101

Ohkubo, I.; Tsubouchi, K.; Kumigashira, H.; Ohnishi, T.; Lippmaa, M.; Matsumoto, Y.; Koinuma, H. & Oshima, M. (2008). Trap-controlled space-chargelimited current mechanism in resistance switching at Al/$Pr_{0.7}Ca_{0.3}MnO_3$ interface. *Appl. Phys. Lett.*, Vol.92, pp. 22113

Pacholski, C.; Kornowski, A. & Weller, H. (2002). Self-assembly of ZnO: from nanodots to nanorods. *Angew. Chem. Int. Ed.*, Vol.41, pp. 1188-1191

Pan, Z. W.; Dai, Z. R. & Wang, Z. L. (2001). Nanobelts of semiconducting oxides. *Science*, Vol.291, pp. 1947-1949

Park, J. Y.; Yun, Y. S.; Hong, Y. S.; Oh, H.; Kim, J.-J. & Kima, S. S. (2005). Synthesis, electrical and photoresponse properties of vertically well-aligned and epitaxial ZnO nanorods on GaN-buffered sapphire substrates. *Appl. Phys. Lett.*, Vol.87, pp. 123108

Park, W.; Jo, G.; Hong, W. K.; Yoon, J.; Choe, M.; Lee, S.; Ji, Y.; Kim, G.; Kahng, Y. H.; Lee, K.; Wang, D. & Lee, T. (2011). Enhancement in the photodetection of ZnO nanowires by introducing surface-roughness-induced traps. *Nanotechnol.*, Vol.22, pp. 205204

Park, W. I.; Kim, D. H.; Jung, S. W. & Yi, G. C. (2002). Metalorganic vapor-phase epitaxial growth of vertically well-aligned ZnO nanorods. *Appl. Phys. Lett.*, Vol.80, pp. 4232–4234

Patra, S.; Satpati, B. & Pradhan, S. K. (2011). Quickest single-step mechanosynthesis of CdS quantum dots and their microstructure characterization. *J. Nanosci. Nanotechnol.*, Vol.11, No.6, pp. 4771-4780

Pearton, S. J.; Norton, D. P.; Ip, K.; Heo, Y. W. & Steiner, T. (2005). Recent progress in processing and properties of ZnO. *Prog. Mater. Sci.*, Vol.50, pp. 293–340

Porter, H. L.; Cai, A. L.; Muth, J. F. & Narayan, J. (2005). Enhanced photoconductivity of ZnO films Co-doped with nitrogen and tellurium. *Appl. Phys. Lett.*, Vol.86, pp. 211918

Pullar, R. C.; Farrah, S. & Alford, N. M. (2007). $MgWO_4$, $ZnWO_4$, $NiWO_4$ and $CoWO_4$ microwave dielectric ceramics. *J. Euro. Cera. Soc.* , Vol.27, pp. 1059-1063

Rose, A. (1955). Space charge limited currents in solids. *Phys. Rev.*, Vol.97, pp. 1538–1544

Soci, C.; Zhang, A.; Xiang, B.; Dayeh, S. A.; Aplin, D. P. R.; Park, J.; Bao, X. Y.; Lo, Y. H. & Wang, D. (2007). ZnO nanowire UV photodetectors with high internal gain. *Nano Lett.* , Vol.7, pp. 1003-1009

Song, J. & Lim, S. (2007). Effect of seed layer on the growth of ZnO nanorods. *J. Phys. Chem. C*, Vol.111, pp. 596-600

Tak, Y. & Yong, K. (2005). Controlled growth of well-aligned ZnO nanorod array using a novel solution method. *J. Phys. Chem. B* Vol.109, pp. 19263-19269

Tsuzuki, T. & McCormick, P. G. (2001). ZnO nanoparticles synthesised by mechanochemical processing. *Scripta Mater.*, Vol.44, pp. 1731-1734

Tsuzuki, T. & McCormick, P. G. (2004). Mechanochemical synthesis of nanoparticles. *J. Mat. Sci.*, Vol.39, pp. 5143-5146

Um, H.-D.; Moiz, S. A.; Park, K.-T.; Jung, J.-Y.; Jee, S.-W.; Ahn, C. H.; Kim, D. C.; Cho, H. K.; Kim, D.-W. & Lee, J.-H. (2011). Highly selective spectral response with enhanced responsivity of n-ZnO/p-Si radial heterojunction nanowire photodiodes *Appl. Phys. Lett.*, Vol.98, pp. 033102

Vayssieres, L. (2003). Growth of arrayed nanorods and nanowires of ZnO from aqueous solutions. *Adv. Mater.*, Vol.15, pp. 464-466

Verges, M. A.; Mifsud, A. & Serna, C. J. (1990). Formation of rodlike zinc-oxide microcrystals in homogeneous solutions. *J. Chem. Soc., Faraday Trans.* , Vol.86, pp. 959-963

Wagner, R. S. & Ellis, W. C. (1964). Vapor-liquid-solid mechanism of single crystal growth. *Appl. Phys. Lett.*, Vol.4, pp. 89-90

Wang, Q. P.; Zhang, D. H.; Xue, Z. Y. & Hao, X. T. (2002a). Violet luminescence emitted from ZnO films deposited on Si substrate by rf magnetron sputtering. *Appl. Surf. Sci.*, Vol.201, pp. 123–128

Wang, Y.; Zhang, L.; Liang, C.; Wang, G. & Peng, X. (2002b). Catalytic growth and photoluminescence properties of semiconductor single-crystal ZnS nanowires. *Chem. Phys. Lett. A*, Vol.357, pp. 314-318

Wei, Y.; Wu, W.; Guo, R.; Yuan, D.; Das, S. & Wang, Z. L. (2010). Wafer-scale high-throughput ordered growth of vertically aligned ZnO nanowire arrays. *Nano Lett.*, Vol.10, pp. 3414-3419

Wu, J. J.; Wen, H. I.; Tseng, C. H. & Liu, S. C. (2004). Well-aligned ZnO nanorods via hydrogen treatment of ZnO films. *Adv. Funct. Mater. Lett.*, Vol.14, pp. 806–810

Wu, W.-Y.; Chen, M.-T. & Ting, J.-M. (2009). Growth and characterizations of ZnO nanorod/film structures on copper coated Si substrates. *Thin Solid Films*, Vol.518, pp. 1549–1552

Wu, Y.; R.Fan & Yang, P. (2002a). Block-by block growth of single-crystalline Si/Si-Ge superlattice nanowires. *Nano Lett.*, Vol.2, pp. 83-86

Wu, Y.; Yan, H.; Huang, M.; Messer, B.; Song, J. H. & Yang, P. (2002b). Inorganic semiconductor nanowires: rational growth, assembly, and novel properties. *Chem. Eur. J.*, Vol.8, pp. 1260-1268

Wu, Y. & Yang, P. (2000). Germanium nanowire growth via simple vapor transport. *Chem. Mater.*, Vol.12, pp. 605-607

Wu, Y. & Yang, P. (2001). Direct observation of vapor-liquid-solid nanowire growth. *J. Am. Chem. Soc.*, Vol.123, pp. 165-166

Xu, S.; Adiga, N.; Ba, S.; Dasgupta, T.; Wu, C. F. J. & Wang, Z. L. (2009). Optimizing and improving the growth quality of ZnO nanowire arrays guided by statistical design of experiments. *ACS Nano*, Vol.3, pp. 1803–1812

Xu, S.; Qin, Y.; Xu, C.; Wei, Y.; Yang, R. & Wang, Z. L. (2010). Self-powered nanowire devices *Nat. Nanotechnol.*, Vol.5, pp. 366-373

Yang, Q.; Xin Guo; Wang, W.; Zhang, Y.; Xu, S.; Lien, D. H. & Wang, Z. L. (2010). Enhancing sensitivity of a single ZnO micro-/nanowire photodetector by piezo-phototronic effect. *ACS Nano*, Vol.4, No.10, pp. 6285-6291

Yao, B. D.; Chan, Y. F. & Wang, N. (2002). Formation of ZnO nanostructures by a simple way of thermal evaporation. *Appl. Phys. Lett.*, Vol.81, pp. 757-759

Yeong, K. S.; H., M. K. & Thong, J. T. L. (2007). The effects of gas exposure and UV illumination on field emission from individual ZnO nanowires. *Nanotechnol.*, Vol.18, pp. 185608

Yuan, H. & Zhang, Y. (2004). Preparation of well-aligned ZnO whiskers on glass substrate by atmospheric MOCVD. . *J. Cryst. Growth*, Vol.263, pp. 119–124

Zhang, Y. J.; Zhang, Q.; Wang, N. L.; Yan, Y. J.; Zhou, H. H. & Zhu, J. (2001). Synthesis of thin Si whiskers (nanowires) using $SiCl_4$. *J. Cryst. Growth & Design*, Vol.226, pp. 185-191

Zhao, D.; Andreazza, C.; Andreazza, P.; Ma, J.; Liu, Y. & Shen, D. (2005). Buffer layer effect on ZnO nanorods growth alignment. *Chem. Phys. Lett.*, Vol.408, pp. 335-338

Zhou, J.; Gu, Y. D.; Hu, Y. F.; Mai, W. J.; Yeh, P. H.; Bao, G.; Sood, A. K.; Polla, D. L. & Wang, Z. L. (2009). Gigantic enhancement in response and reset time of ZnO UV nanosensor by utilizing Schottky contact and surface functionalization. *Appl. Phys. Lett.*, Vol.94, pp. 191103